Applied Physics Letters

Polarization switching in $Hf_{0.5}Zr_{0.5}O_2$-dielectric stack: The role of dielectric layer thickness

Cite as: Appl. Phys. Lett. **119**, 122903 (2021); https://doi.org/10.1063/5.0056448
Submitted: 10 May 2021 • Accepted: 03 September 2021 • Published Online: 24 September 2021

Atanu K. Saha, Mengwei Si, Peide D. Ye, et al.

Applied Physics Letters ARTICLE scitation.org/journal/apl

Polarization switching in $Hf_{0.5}Zr_{0.5}O_2$-dielectric stack: The role of dielectric layer thickness

Cite as: Appl. Phys. Lett. **119**, 122903 (2021); doi: 10.1063/5.0056448
Submitted: 10 May 2021 · Accepted: 3 September 2021 ·
Published Online: 24 September 2021

View Online Export Citation CrossMark

Atanu K. Saha,[a] Mengwei Si, Peide D. Ye, and Sumeet K. Gupta

AFFILIATIONS

School of Electrical and Computer Engineering, Purdue University, West Lafayette, Indiana 47907, USA

[a]Author to whom correspondence should be addressed: saha26@purdue.edu

ABSTRACT

Understanding the role of the dielectric (DE) layer in ferroelectric (FE) $Hf_{0.5}Zr_{0.5}O_2$ (HZO) based devices (e.g., ferroelectric-field-effect-transistors, FE-FETs) is important to enable their application-driven optimizations. To that end, in this work, we systematically investigate the polarization switching mechanisms in FE–DE stacks and analyze their dependence on the dielectric layer thickness (T_{DE}). First, we fabricate a HZO–Al_2O_3 (FE–DE) stack and experimentally demonstrate a decrease in remanent polarization and an increase in coercive voltage with an increase in T_{DE}. As such dependencies are out of the scope of commonly used single domain polarization switching models, therefore, we argue that the consideration of the multi-domain model is essential for analyzing the polarization switching in HZO. Then, using phase-field simulations of the FE–DE stack, we show that an increase in T_{DE} results in a larger number of reverse domains in the FE layer to suppress the depolarization field, which leads to a decrease in the remanent polarization and an increase in the coercive voltage. Furthermore, our analysis signifies that the polarization switching mechanism in HZO can be modulated from domain-nucleation based to domain-wall motion based by increasing the T_{DE} and that can serve as a potential knob for application-specific optimization of FE-FETs. In addition, we show that the effective polarization–voltage characteristics of the FE layer in the FE–DE stack exhibit a negative slope region that leads to the charge enhancement effects in the FE–DE stack. While such effects are most commonly misinterpreted as either the transient effects or the stabilized single-domain negative capacitance effects, we demonstrate that the appearance of a negative slope in the hysteretic polarization–voltage characteristics is quasi-static in nature and that originates from the multi-domain polarization switching in the FE.

Ferroelectric (FE) hafnium-zirconium-oxide (HZO), by virtue of its CMOS process compatibility[1,2] and rich domain dynamics,[3,4] has been identified as one of the most promising candidates for future electronic devices. By integrating HZO as the FE layer in the gate stack of a transistor (ferroelectric-field-effect-transistors, FE-FET), nonvolatile memory (NVM),[5,6] neurons,[7] and synaptic[8,9] functionalities have been demonstrated. Such diverse functionalities demand different characteristics of polarization (P) switching in the HZO layer. For example, an abrupt P-switching is beneficial for neurons and binary NVMs, while a gradual P-switching is favorable for multi-bit memories and synapses. Therefore, it becomes essential to appropriately design FE-FETs for application-specific device behavior, for which gate stack optimization plays a key role. In the FE-FET gate stack, a dielectric (DE) layer exists between the FE and the semiconductor channel,[5–10] which can significantly impact the FE-FET characteristics.[11] According to the single-domain (SD) Landau–Khalatnikov (LK) model of FE, an increase in the DE thickness (T_{DE}) should increase the depolarization field and reduce the coercive voltage (V_C) of the FE–DE stack[12,13] (see the supplementary material). However, the FE–DE stack with HZO as the FE and Al_2O_3/HfO_2 as the DE layer have been demonstrated[14,15] to exhibit an increasing coercive voltage (V_C) with the increase in T_{DE}. Therefore, it is important to bridge the gap between the theoretical understanding and experimental observations regarding the role of the DE layer thickness in the P-switching characteristics of FE HZO.[12,13] To that end, in this Letter, we experimentally and theoretically analyze the P-switching in the FE–DE stack with HZO as the FE and Al_2O_3 as the DE layer. Our results signify an increase in V_C, a decrease in remanent-P (P_R), and a decrease in the P-switching slope with the increase in T_{DE}. By employing phase-field simulations, we show that such dependencies can be attributed to the multi-domain (MD) phenomena in FE,[16] which cannot be captured in the single-domain P-switching model.[12] To further study the role of the DE layer, we analyze the dependence of V_C, P_R, and the switching slope of the FE–DE stack through phase-field simulations. It is worth noting that while the multi-domain formation in FE in the presence of a dead layer and in FE–DE stack is a well-explored topic in the context of perovskite-based FE, the considered HZO–Al_2O_3 system and the corresponding analysis in this paper are significantly different. For instance, the fundamental nature of P-switching dynamics in FE HZO (fluorite based) is expected to be significantly different from the perovskite-based FE materials [i.e., lead zirconate titanate (PZT), barium titanate (BTO), etc.] because of the substantially less elastic coupling in the fluorites compared to the perovskites.[22] In addition, the previous works[26–30] were mostly focused on the temperature-driven phase transition and the dependence of the domain configuration on stress and other factors. In contrast, in our work, we focus on the applied voltage-driven polarization switching and the influence of microscopic interactions (electrostatic and elastic) and how the DE thickness plays an important role to modulate the multi-domain configuration and, thus, the corresponding P-switching mechanism.

For fabrication of the FE–DE stacks, we start with standard solvent cleaning of heavily p-doped Si substrates. Then, a 30 nm TiN layer is deposited by atomic layer deposition (ALD) at 250 °C, using $[(CH_3)_2N]_4Ti$ and NH_3 as the Ti and N precursors, respectively. After this, an HZO film is deposited by ALD at 200 °C, using $[(CH_3)_2N]_4Hf$, $[(CH_3)_2N]_4Zr$, and H_2O as the Hf, Zr, and O precursors, respectively. A HfO_2:ZrO_2 cycle ratio of 1:1 is used to form the 10 nm $Hf_{0.5}Zr_{0.5}O_2$ film. Similarly, on top of HZO, an Al_2O_3 layer is deposited followed by 30 nm TiN layer deposition. After that, the samples are annealed at 500 °C in the N_2 environment for 1 minute by rapid thermal annealing. Then, Ti/Au top electrodes are fabricated using photolithography, e-beam evaporation, and lift-off process (area = 5024 μm^2). The material level characterization of the HZO and HZO–Al_2O_3 stacks (i.e., XRD and SEM/TEM) can be found in Refs. 31 and 32. The average polarization (P_{avg}) vs applied voltage (V_{app}) measurement is carried out using a Radiant RT66C FE tester at room temperature at a very low frequency (50 Hz). Considering the polarization switching time in HZO ($<1\,\mu s$),[17] such low-frequency measurements can be considered as quasi-static. Figure 1(a) shows the P_{avg}–V_{app} characteristics of the FE–DE stack for 10 nm HZO and 1/3/5 nm Al_2O_3. Our results show a decrease in P_R (P_{avg} at $V_{app} = 0$ V), an increase in V_C (V_{app} at $P_{avg} = 0$), and a decrease in the P-switching slope (dV_{avg}/dV_{app}) with the increase in T_{DE}. To explain such dependencies, we now analyze the P-switching in the FE–DE stack based on multi-domain phase-field simulation.

In our 2D phase-field simulation,[18,19] we self-consistently solve the time-dependent Ginzburg–Landau (TDGL) equation [Eq. (1)] and Poisson's equation [Eq. (2)] in 2D space (xz plane) employing the finite difference method,

$$-\frac{1}{\Gamma}\frac{\partial P}{\partial t} = \alpha P + \beta P^3 + \gamma P^5 - g_{11}\frac{d^2P}{dz^2} - g_{44}\frac{d^2P}{dx^2} + \frac{d\phi}{dz}, \quad (1)$$

$$-\epsilon_0\left[\frac{\partial}{\partial x}\left(\epsilon_x\frac{\partial\phi}{\partial x}\right) + \frac{\partial}{\partial z}\left(\epsilon_z\frac{\partial\phi}{\partial z}\right)\right] = -\frac{dP}{dz}. \quad (2)$$

Here, α, β, and γ are Landau coefficients; $g_{11(44)}$ is the gradient coefficient; $\epsilon_{z(x)}$ is the relative background permittivity; Γ is the

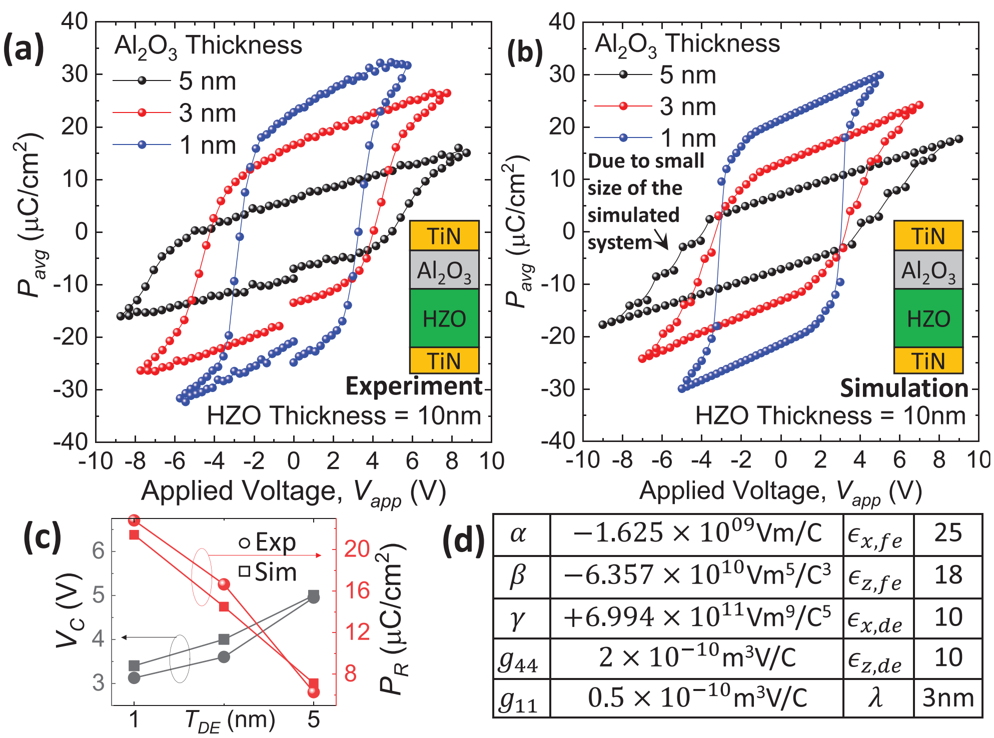

α	-1.625×10^{09}Vm/C	$\epsilon_{x,fe}$	25
β	-6.357×10^{10}Vm^5/C^3	$\epsilon_{z,fe}$	18
γ	$+6.994 \times 10^{11}$Vm^9/C^5	$\epsilon_{x,de}$	10
g_{44}	2×10^{-10}m^{3}V/C	$\epsilon_{z,de}$	10
g_{11}	0.5×10^{-10}m^{3}V/C	λ	3nm

FIG. 1. (a) Measured and (b) simulated P_{avg}–V_{app} characteristics of FE–DE stacks for different T_{DE}. (c) Average V_C (V_{app} at $P_{avg} = 0$) and P_R (P_{avg} at $V_{app} = 0$) for different T_{DE}. (d) Table showing the simulation parameters.

viscosity coefficient; ϕ is the potential; and P is the local polarization of an FE unit cell. We assume that the P-direction (c-axis of the orthorhombic HZO crystal) is parallel to the film thickness (z-axis).[18–22] Note that the dP/dz induces charges in the FE layer and, thus, enters in Eq. (2). At the FE–DE interface, $\lambda(dP/dz)-P=0$ is used for the surface energy contribution, where λ is the extrapolation length.[20,21] All simulation parameters are given in Fig. 1(d) that we obtain from our previous work[22] by calibrating the phase-field model with experimental characteristics of the HZO–Al_2O_3 stack with different HZO thicknesses. Due to the non-centrosymmetric crystal and lower elastic interactions in the out-of-plane direction compared to the in-plane direction in HZO,[23] we use $g_{11} < g_{44}$. Similarly, as the P-direction is along the z-axis, therefore, a lower number of atoms per unit cell take part in determining ϵ_z compared to ϵ_x and hence, $\epsilon_z < \epsilon_x$ (which is similar to other FE like PZT[24]). We consider the length (l, along the x-direction) of the system to be 30 nm, which is similar to the average grain size of HZO.[25] To be consistent with the experimental measurements, simulations are performed based on the quasi-static criteria (negligible dP/dt). Therefore, our simulation results are independent of the value of Γ. Furthermore, we use a smaller FE region (equivalent to the size of a grain $\sim$30 nm) in simulation compared to the area of our experimental sample because of the scale-free nature of the FE HZO.[22] Thus, our simulations capture the trends with respect to the mean behavior of a single grain; however, for capturing the effects such as variation in coercive fields, a multi-grain simulation is needed, which is outside of scope of this work. In the multi-domain scenario, the P_{avg} is computed by integrating the displacement field at the metal–DE (or metal–FE) interface $\{P_{avg}=(\int \epsilon_0\epsilon_{z,DE}E_{z,DE}dx)/l=[\int(P+\epsilon_0\epsilon_{z,FE}E_{z,FE})dx]/l\}$. Here, the $E_{z,FE(DE)}$ is the out-of-plane (z) component of the electric field in the FE (DE) layer. It is noteworthy that the P_{avg} not only contains the average spontaneous P but also includes the induced displacement field, and therefore, P_{avg} effectively represents the average out-of-plane displacement field in the FE–DE stack. The simulated P_{avg}–V_{app} characteristics of the FE–DE stack are shown in Fig. 1(b), illustrating a good agreement with the experiments [Fig. 1(c)]. The mismatch in the P-switching region can be reduced by simulating multiple grains (discussed later).

To explain these characteristics, let us start with $V_{app}=0$ V and $P_R<0$. In an FE–DE stack, the P-induced bound charges appear near the FE–DE interface leading to a non-zero $E_{z,DE}$, and $E_{z,FE}$. If P is homogeneous [e.g., in a single-domain (SD) state], then $E_{z,FE}$ will be directed opposite to the P-direction yielding depolarization energy f_{dep} $(=-PE_{z,FE})$. At the same time, $E_{z,FE}$ will reduce the P magnitude ($|P|$) leading to an increase in the free energy (f_{free}). In order to suppress f_{dep} and f_{free} (to minimize the overall energy), FE breaks into multiple domains with opposite P-directions. In this multi-domain (MD) state, the P-induced bound charges at the FE–DE interface not only give rise to $E_{z,FE(DE)}$ (as before) but also form the in-plane E-field [$E_{x,FE(DE)}$] called a stray field.[18,26] As a portion of the bound charge gets compensated by the stray-field, $E_{z,FE(DE)}$ is reduced in the MD state (compared to the SD state), leading to a higher local P. This results in a reduction in f_{dep} and f_{free}. However, this suppression of f_{dep} and f_{free} occurs at the cost of (i) gradient energy, f_{grad} $[=g_{44}(dP/dx)^2]$ due to the spatial variation of P near the domain-walls (DWs) and (ii) electrostatic energy f_{elec} $(=\epsilon_0\epsilon_{x,FE}E_{x,FE}^2)$ due to the stray fields. Hence, the formation of the MD state in FE occurs as an interplay among competing energy components to obtain the minimum energy for the whole system. With this understanding, let us now discuss the impact of T_{DE} on P_R.

In the FE–DE stack (at $V_{app}=0$ and $P_R<0$), an increase in T_{DE} tends to increase $E_{z,FE}$ due to the higher voltage drop across DE and an equal and opposite voltage drop across the FE layer. This increase in $E_{z,FE}$ tends to increase f_{dep} and f_{free}. To counter this, a larger number of oppositely polarized domains ($+P$ in Fig. 2) appear that create more stray fields to suppress $E_{z,FE}$. The simulated P and E-field profiles in Figs. 2(a)–2(c) validate the increase in the number of $+P$ domains (red domains) and suppression of $E_{z,FE}$ [Fig. 2(d)] with the increase in T_{DE}. The appearance of a larger number of $+P$ domains leads to smaller $-P$ domains (blue) and, hence, reduced $|P_R|$ with the increase in T_{DE} [Figs. 1(a)–1(c)].

Now, let us discuss V_{app}-induced P-switching. In the MD scenario, the P-switching can take place locally if $f_{grad}+f_{dep}+f_{elec}+f_{\mathrm{free}}>\max(f_{free})$. Therefore, for this discussion of local P-switching, we will use the notion of local electric-fields and energy components. First, note that the local $E_{z,FE}$ is maximum away from DW near the FE–DE interface, which leads to maximum f_{dep}. In contrast, f_{grad} is maximum near the DW due to the largest variation in P at the DW. Now, with an increase in V_{app} (>0 V), the local (depolarizing) $|E_{z,FE}|$ increases in $-P$ domains and decreases in $+P$ domains leading to a local change in the P magnitude ($|P|$ decreases in $-P$ domains and increases in $+P$ domains). This V_{app} induced local change in $E_{z,FE}$ and P yields an increase in $f=f_{grad}+f_{dep}+f_{elec}+f_{\mathrm{free}}$ in the $-P$ domains.[16] If the increase in f is dominant near the DW, then P-switching occurs through DW motion. However, if the increase in f is dominant away from the DW, then P-switching occurs through the nucleation of new domains. P profiles at different V_{app} are shown in Fig. 3(a-i) for $T_{DE}=1$ nm. With the increase in V_{app}, P-switching starts through DW motion (at $V_{app}=1.5$ V) and at $V_{app}>3$ V several new domains nucleate causing a denser domain pattern. The transient nature of domain nucleation is shown in Fig. 3(a-ii), signifying their formation starting from the FE–DE interface and a little away from the existing DW. Once, the domain pattern becomes denser, a significant portion of $E_{z,FE}$ is suppressed by the stray fields, albeit at the expense of some increase in f_{grad}. In this case, the maximum of f occur near the DW, and hence, with further increase in V_{app}, P-switching takes place through DW motion leading to complete switching ($-P$ to $+P$) of several reverse domains. Similarly, for $T_{DE}=3$ nm [Figs. 3(b-i) and 3(b-ii)], P-switching initiates through DW motion (at $V_{app}=1.85$ V) followed by domain nucleation (at $V_{app}>3.15$ V) and then DW motion. However, for $T_{DE}=5$ nm [Fig. 3(c)], the initial domain pattern is much denser, which suppresses $E_{z,FE}$ at the cost of a increased f_{grad}. Hence, nucleation of new domains is not observed, and P-switching takes place only through DW motion (at $V_{app}>3.6$ V). It is important to note that, for both the domain-nucleation and DW motion we discussed here, the increase in f_{dep} (or an increase in depolarizing $E_{z,FE}$) is the dominant component for satisfying the P-switching condition, $f>\max(f_{free})$. This is because the f_{grad} component is significantly less in HZO (due to a lower gradient energy coefficient compared to the conventional perovskite-based FE materials). As f_{dep} is the dominant energy component for the P-switching in HZO, hence, there is a correlation between the domain nucleation and DW-motion. For instance, the DW-motion in HZO can be thought of as the nucleation of a region just in the vicinity of the DW.

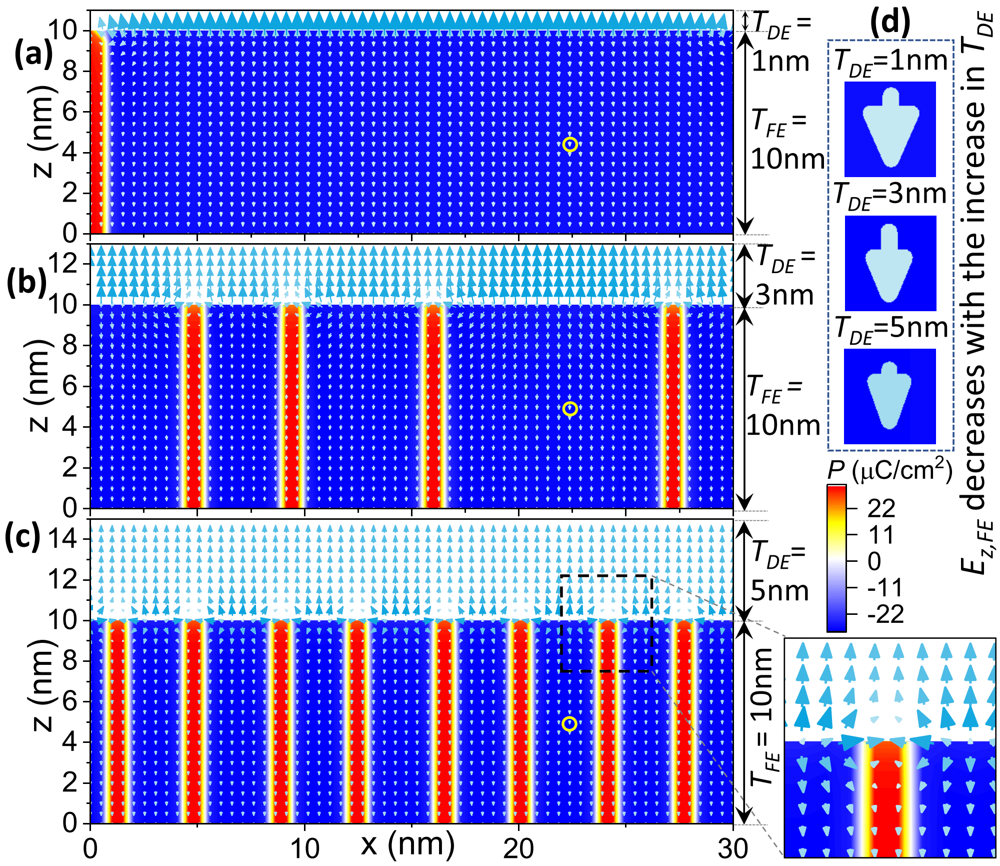

FIG. 2. Simulated P (color map) and E-field (arrow) profile in FE–DE stacks for T_{DE} = (a) 1 nm, (b) 3 nm, and (c) 5 nm. The blue (red) regions signifying $-P$ ($+P$) domains. (d) $E_{z,FE}$ at the yellow circled points shown in (a)–(c) signifying the decrease in the depolarization field within the FE with the increase in DE due to the formation of a larger number of reverse domains.

Now, let us analyze the effective polarization–voltage characteristics of the FE layer in the FE–DE stack. To obtain the average voltage drop across the FE layer (V_{FE}) for a particular P_{avg}, we compute the average voltage drop across the DE layer (V_{DE}) from its capacitance ($C_{DE} = \epsilon_0 \epsilon_{r,DE}/T_{DE}$) and displacement continuity condition ($V_{DE} = P_{avg}/C_{DE}$). Then, we compute the V_{FE} ($=V_{APP}-V_{DE}$) and plot the P_{avg}–V_{FE} curves from both experimental and simulated characteristics as shown in Figs. 4(a) and 4(b). It should be noted that these P_{avg}–V_{FE} characteristics are not an explicit or intrinsic representation of the P_{avg}–V_{FE} characteristics of a standalone FE layer. Rather, this is an effective and/or apparent representation of P_{avg}–V_{FE} characteristics of the FE layer that appears in an FE–DE stack. It is interesting to note that these extracted P_{avg}–V_{FE} characteristics signify a negative dP_{avg}/dV_{FE} region during the multi-domain P-switching in the FE layer, which is similar to the earlier works on perovskite-based FE.[35–37] While such effects have been interpreted in some earlier works as either the transient effects[13] or the stabilized single-domain negative capacitance effects,[34] here our simulations suggest that the appearance of the negative slope in the hysteretic P_{avg}–V_{FE} characteristics are quasi-static in nature originating from the multi-domain P- switching in the FE layer. To understand the physical origin of this negative P_{avg}–V_{FE} slope, first, recall that the local (and average) $E_{z,FE}$ in the FE layer is depolarizing, i.e., opposite to the direction of local and average P. Now, let us consider the FE–DE stack is in the $P_R < 0$ states (average $E_{z,FE} > 0$). When V_{app} is increased (>0 V) and leads to MD P-switching, the P_{avg} increases either through the formation of new $+P$ domains (nucleation) or through the size increase in $+P$ domains (DW displacement). Both of these phenomena lead to a large decrease in local $E_{z,FE}$ (from positive to negative) in the newly switched $+P$ region leading to a decrease in average $E_{z,FE}$ (i.e., the average $E_{z,FE}$ becomes less positive). As the increase in P_{avg} accompanies the decrease in average V_{FE} ($=T_{FE}E_{z,FE}$), thus the dP_{avg}/dV_{FE} becomes negative. A similar negative dP_{avg}/dV_{FE} region can be obtained for $P_R > 0$ and $V_{app} < 0$. It is important to note that the appearance of negative dP_{avg}/dV_{FE} is an electrostatic effect as each of the points in the P_{avg}–V_{FE} curve is electrostatically stable. However, the actual slope of dP_{avg}/dV_{FE} can certainly be impacted by the frequency of the applied V_{app} due to the time-dependency of domain-nucleation and DW-motion. Moreover, the P_{avg}–V_{FE} characteristics are not independent of T_{DE} [Fig. 4(a)], and hence, the possibilities for single domain P-switching to be the source of negative dP_{avg}/dV_{FE} are unlikely in this considered scenario.

Further, the DW motion occurs via lattice-by-lattice propagation yielding a gradual increase in P_{avg}. In contrast, nucleation of a

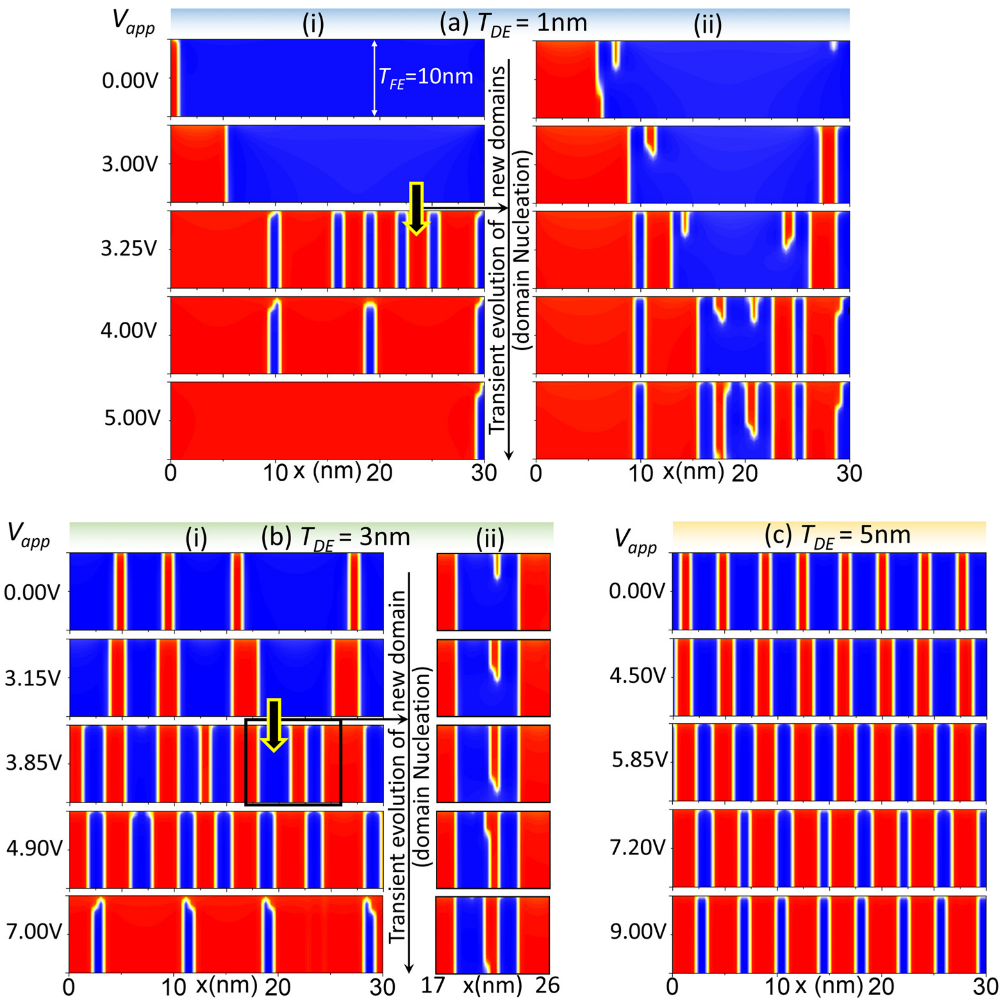

FIG. 3. Simulated polarization profile in FE at different applied voltages (V_{app}) in FE–DE stacks for different T_{DE} = (a) 1 nm, (b) 3 nm, and (c) 5 nm showing domain nucleation and domain-wall motion-based polarization switching. In all the cases, the FE thickness is 10 nm.

new domain involves simultaneous P-switching in several lattices leading to a sharper change in P_{avg}. Since, with an increase in T_{DE}, the dominant P-switching mechanism changes from nucleation to DW-motion-based, P-switching becomes more gradual—Figs. 1(a) and 1(b). Furthermore, our simulations show a stepwise P-switching behavior for $T_{DE} = 5$ nm [Fig. 1(b)], where each step jump signifies the DW displacement, and the flatter region corresponds to no DW displacement. The non-zero slope of the flatter region is due to the background permittivity and the change in P magnitude. In this flat region, with an increase in V_{app}, $E_{z,FE}$ first increases. If the increase in $E_{z,FE}$ is beyond a critical value so that $f > \max(f_{free})$, then the P-switching takes place via DW displacement. Recall that the P-switching leads to an increase in P_{avg} and a simultaneous reduction in $E_{z,FE}$. This yields a negative slope in the P_{avg}–V_{FE} characteristics ($dP_{avg}/dV_{FE} < 0$) and a step jump in the P_{avg}–V_{app} characteristics. Now, after each P-switching step, to induce further DW motion, V_{app} needs to be increased to increase $E_{z,FE}$ beyond a (new) critical value. Consequently, we observe a stepwise P-switching behavior in Figs. 1(b) and 4(b). However, such step-jumps are absent in the measured characteristics because of the larger area (lots of grains) of the fabricated sample compared to our simulation (∼one grain). Thus, even though the DW motion may be absent in some of the grains of the experimental sample, it may be present in other grains (due to the variation in grain size and/or crystallographic angle) leading to a continuous increase in P_{avg} and decrease in $E_{z,FE}$. Hence, we expect that simulation of a larger system considering multiple grains may reduce this mismatch between the simulation and experimental results.

Let us now explain the effect of T_{DE} on the average coercive voltage, V_C (defined as the V_{app}, where $P_{avg} = 0$). For that, we use the notion of the average voltage drop across the FE layer (V_{FE}). As an increase in T_{DE} and corresponding formation of the denser domain pattern in the FE layer suppress the local and average $E_{z,FE}$ (discussed before), it leads to a decrease in V_{FE} at $V_{app} = 0$ V. With the decrease

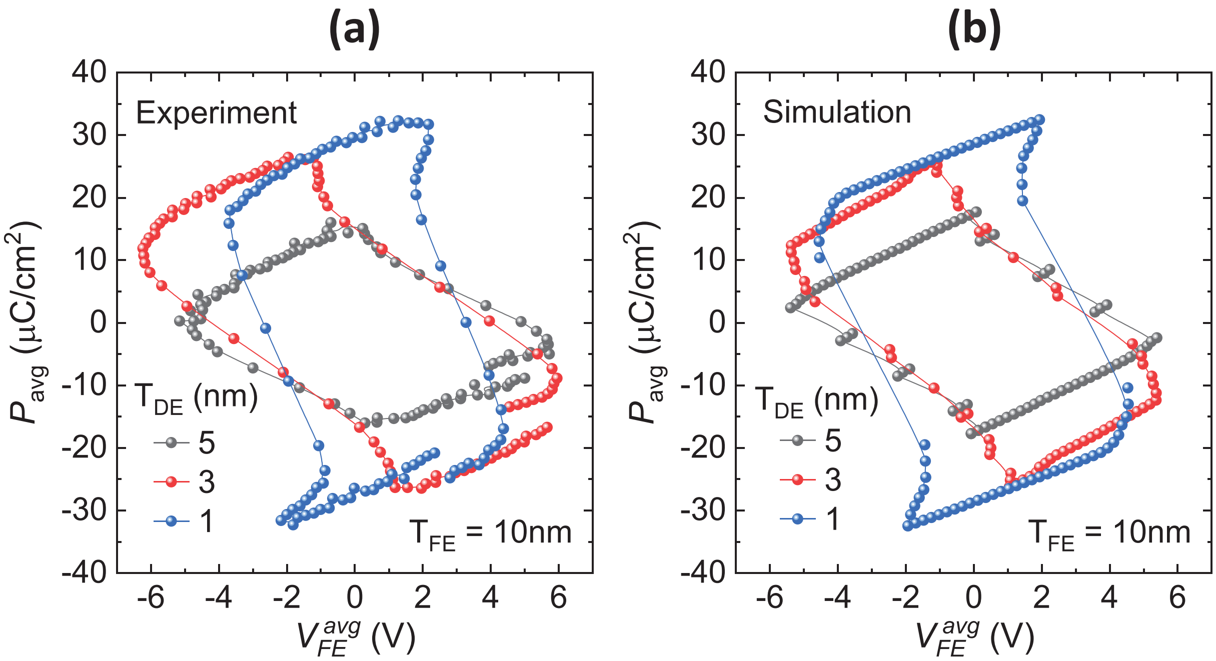

FIG. 4. Extracted average polarization (P_{avg}) vs average voltage across the FE layer (V_{FE}) in the FE–DE stack from the (a) experimental and (b) simulated P_{avg}–V_{app} characteristics.

in initial V_{FE}, a higher V_{app} is required to achieve a critical V_{FE} (as well as local $E_{z,FE}$) to trigger P-switching. Therefore, the DW motion initiates at $V_{app} = 1.5$ V for $T_{DE} = 1$ nm and at 1.85 V for $T_{DE} = 3$ nm. Similarly, the domain nucleation takes place at $V_{app} > 3$ V for $T_{DE} = 1$ nm and $V_{app} > 3.15$ V for $T_{DE} = 3$ nm. Furthermore, dP_{avg}/dV_{app} decreases with the decrease in T_{DE} (discussed before) leading to an increase in required V_{app} to achieve $P_{avg} = 0$. Due to the decrease in initial V_{FE} (at $V_{app} = 0$ V) and lower dP_{avg}/dV_{app}, V_C of the FE–DE stack increases with an increase in T_{DE}. Note that the increase in V_C for larger T_{DE} cannot be captured by the SD model[12] but can be described well considering the MD effects (as explained above).

So far, we have discussed different attributes of P_{avg}–V_{app} characteristics of FE–DE stacks with respect to different T_{DE}. This can also be regarded as the influence of different DE capacitances ($C_{DE} = \epsilon_0\epsilon_{DE}/T_{DE}$) in the FE-DE stack. Now, one may argue that the P_{avg}–V_{app} characteristics can be tuned similarly by using a different DE material (ϵ_{DE}). While this is indeed possible (and can be an important design knob), the effect of ϵ_{DE} is not just changing C_{DE} but involves some more physical processes that mandate further analysis. To decouple the effect of ϵ_{DE} on C_{DE}, we theoretically analyze the FE–DE characteristics in the supplementary material by simultaneously and proportionally changing ϵ_{DE} and T_{DE} to keep the same C_{DE}. We show that the P_{avg}–V_{app} characteristics are not unique to C_{DE}, rather they depend on the choice of ϵ_{DE}. Such dependency originates due to the electrostatic boundary condition of the in-plane electric field at the FE–DE interface. Considering different ϵ_{DE} (but the same C_{DE}), our simulation results suggest that the V_C decreases and P_R increases with the decrease in ϵ_{DE}. We discuss such an ϵ_{DE} dependency on the P-switching in the FE–DE stack in the supplementary material.

In summary, we show that the FE layer forms a denser domain pattern with increasing T_{DE} by suppressing the depolarization field and leading to a larger hysteresis in the FE–DE stack. Simultaneously, the mechanism of P-switching can be modulated from nucleation to DW-motion dominant by increasing T_{DE}. In addition, we show that the coercive voltage and remanent polarization can further be modulated by ϵ_{DE} while keeping the same C_{DE}. Such T_{DE} and ϵ_{DE} dependency can serve as the potential knobs to deploy the application-driven optimization of the FE-FET gate stack. For instance, FE-FETs with low T_{DE} (high switching slope) can be used for the design of binary NVMs and neurons, while high T_{DE} can be utilized for multi-bit memories and synapse designs.

See the supplementary material for the P-switching characteristics in the FE–DE stack (i) with the single-domain approximation and (ii) the impact of dielectric permittivity on multi-domain P-switching.

This work was supported in part by Semiconductor Research Corporation (SRC) under Contract No. 2020-LM-2959 and the National Science Foundation (NSF) under Grant Nos. 1814756 and 2008412.

DATA AVAILABILITY

The data that support the findings of this study are available from the corresponding author upon reasonable request.

REFERENCES

[1]J. Müller, T. S. Böscke, S. Müller, E. Yurchuk, P. Polakowski, J. Paul, D. Martin, T. Schenk, K. Khullar, A. Kersch, W. Weinreich, S. Riedel, K. Seidel, A. Kumar,

T. M. Arruda, S. V. Kalinin, T. Schlösser, R. Boschke, R. van Bentum, U. Schröder, and T. Mikolajick, in *IEDM Technical Digest* (IEEE, 2013), pp. 10.8.1–10.8.4.
[2]A. K. Saha, B. Grisafe, S. Datta, and S. K. Gupta, in *Proceedings of the IEEE VLSI Technology* (IEEE, 2017), pp. T226–T227.
[3]K. Ni, B. Grisafe, W. Chakraborty, A. K. Saha, S. Dutta, M. Jerry, J. A. Smith, S. Gupta, and S. Datta, in *IEDM Technical Digest* (IEEE, 2018), pp. 16.1.1–16.1.4.
[4]A. K. Saha, K. Ni, S. Dutta, S. Datta, and S. Gupta, Appl. Phys. Lett. **114**(20), 202903 (2019).
[5]K. Chatterjee, S. Kim, G. Karbasian, A. J. Tan, A. K. Yadav, A. I. Khan, C. Hu, and S. Salahuddin, IEEE Electron Device Lett. **38**(10), 1379–1382 (2017).
[6]S. Dünkel, M. Trentzsch, R. Richter, P. Moll, C. Fuchs, O. Gehring, M. Majer, S. Wittek, B. M. T. Melde, H. Mulaosmanovic, S. Slesazeck, S. Müller, J. Ocker, M. Noack, D.-A. Löhr, P. Polakowski, J. Müller, T. Mikolajick, J. Höntschel, B. Rice, J. Pellerin, and S. Beyer, in *IEDM Technical Digest* (IEEE, 2017), pp. 19.7.1–19.7.4.
[7]H. Mulaosmanovic, E. Chicca, M. Bertele, T. Mikolajickac, and S. Slesazecka, Nanoscale **10**(46), 21755–21763 (2018).
[8]H. Mulaosmanovic, J. Ocker, S. Müller, M. Noack, J. Müller, P. Polakowski, T. Mikolajick, and S. Slesazeck, in *IEEE VLSI Technology* (IEEE, 2017), pp. T176–T177.
[9]M. Jerry, P. Chen, J. Zhang, P. Sharma, K. Ni, S. Yu, and S. Datta, in *IEDM Technical Digest* (IEEE, 2017), pp. 6.2.1–6.2.4.
[10]P. Sharma, K. Tapily, A. K. Saha, J. Zhang, A. Shaughnessy, A. Aziz, G. L. Snider, S. Gupta, R. D. Clark, and S. Datta, in *IEEE VLSI Technology* (IEEE, 2017), pp. T154–T155.
[11]V. Gaddam, D. Das, and S. Jeon, IEEE Trans. Electron Devices **67**(2), 745–750 (2020).
[12]S. Salahuddin and S. Datta, Nano Lett. **8**(2), 405–410 (2007).
[13]A. K. Saha, S. Datta, and S. Gupta, J. Appl. Phys. **123**(10), 105102 (2018).
[14]W. Xiao, C. Liu, Y. Peng, S. Zheng, Q. Feng, C. Zhang, J. Zhang, Y. Hao, M. Liao, and Y. Zhou, IEEE Electron Device Lett. **40**(5), 714–717 (2019).
[15]M. Si, X. Lyu, and P. D. Ye, ACS Appl. Electron. Mater. **1**(5), 745–751 (2019).
[16]A. M. Bratkovsky and A. P. Levanyuk, "Abrupt appearance of the domain pattern and fatigue of thin ferroelectric films," AIP Conf. Proc. **535**(1), 218–228 (2000).
[17]M. Si, X. Lyu, P. R. Shrestha, X. Sun, H. Wang, K. P. Cheung, and P. D. Ye, Appl. Phys. Lett. **115**(7), 072107 (2019).
[18]A. K. Saha and S. K. Gupta, Sci. Rep. **10**(1), 10207 (2020).
[19]H. W. Park, J. Roh, Y. B. Lee, and C. S. Hwang, Adv. Mater. **31**(32), 1805266 (2019).
[20]M. D. Glinchuk and E. A. Eliseev, J. Appl. Phys. **93**(2), 1150 (2003).
[21]P. Chandra and P. B. Littlewood, *Physics of Ferroelectrics: A Modern Perspective*, Topics Applied Physics Vol. 105, edited by K. Rabe, C. H. Ahn, and J.-M. Triscone (Springer-Verlag, Berlin, 2007), pp. 69–116.
[22]A. K. Saha, M. Si, K. Ni, S. Datta, P. D. Ye, and S. K. Gupta, in *IEEE International Electron Devices Meeting (IEDM)* (IEEE, 2020), pp. 4.3.1–4.3.4.
[23]H.-J. Lee, M. Lee, K. Lee, J. Jo, H. Yang, Y. Kim, S. C. Chae, U. Waghmare, and J. H. Lee, Science **369**(6509), 1343–1347 (2020).
[24]A. I. Kurchak, E. A. Eliseev, S. V. Kalinin, M. V. Strikha, and A. N. Morozovska, Phys. Rev. Appl. **8**(2), 024027 (2017).
[25]H. J. Kim, M. H. Park, Y. J. Kim, Y. H. Lee, W. Jeon, T. Gwon, T. Moon, K. D. Kim, and C. S. Hwanga, Appl. Phys. Lett. **105**(19), 192903 (2014).
[26]J. Íñiguez, P. Zubko, I. Luk'yanchuk, and A. Cano, Nat. Rev. Mater. **4**(4), 243–256 (2019).
[27]M. B. Okatan, A. L. Roytburd, J. V. Mantese, and S. P. Alpay, "Domain engineering in compositionally graded ferroelectric films for enhanced dielectric response and tunability," J. Appl. Phys. **105**, 114106 (2009).
[28]M. B. Okatan, J. V. Mantese, and S. P. Alpay, "Polarization coupling in ferroelectric multilayers," Phys. Rev. B **79**, 174113 (2009).
[29]M. B. Okatan, M. W. Cole, and S. P. Alpay, "Dielectric tunability of graded barium strontium titanate multilayers: Effect of thermal strains," J. Appl. Phys. **104**, 104107 (2008).
[30]A. L. Roytburd, S. Zhong, and S. P. Alpay, "Dielectric anomaly due to electrostatic coupling in ferroelectric-paraelectric bilayers and multilayers," Appl. Phys. Lett. **87**(9), 092902 (2005).
[31]S. Zhong, S. P. Alpay, and J. V. Mantese, "High capacity oxide/ferroelectric/oxide stacks for on-chip charge storage," Appl. Phys. Lett. **89**(4), 042906 (2006).
[32]X. Lyu, M. Si, X. Sun, M. A. Capano, H. Wang, and P. D. Ye, in *2019 Symposium on VLSI Technology* (IEEE, 2019), pp. T44–T45.
[33]S. Im, S.-Y. Kang, Y. Kim, J. H. Kim, J.-P. Im, S.-M. Yoon, S. E. Moon, and J. Woo, Micromachines **11**, 910 (2020).
[34]M. Hoffmann, F. P. G. Fengler, M. Herzig, T. Mittmann, B. Max, U. Schroeder, R. Negrea, P. Lucian, S. Slesazeck, and T. Mikolajick, Nature **565**, 464–467 (2019).
[35]A. Kopal, P. Mokrý, J. Fousek, and T. Bahník, Ferroelectrics **223**, 127–134 (1999).
[36]A. M. Bratkovsky and A. P. Levanyuk, Phys. Rev. B **63**, 132103 (2001).
[37]A. M. Bratkovsky and A. P. Levanyuk, Appl. Phys. Lett. **89**, 253108 (2006).